Chapter 4

Modelling Accretion on to Protostellar Systems

In Chapters 5 and 6 of this thesis, the effects of accretion on a protobinary system during its formation is studied. Before this is done, however, a method for representing the protostars in Smoothed Particle Hydrodynamics must be developed. The problem of including protostars in SPH is part of the wider problem of being able to model a large range in length, density and dynamic time scales using any numerical method.

4.1 Problems of Modelling Multiple Star Formation

As an example of the problem, consider binary star formation, which is directly related to the work in this thesis. As discussed in the introduction to this thesis (Chapter 1), the majority of stars are in binary or multiple systems. A possible mechanism to explain the formation of most binary and multiple systems is fragmentation - either standard or disc fragmentation, or a combination of the two (Sections 1.3.3 and 1.3.4).

Unfortunately, numerical calculations of fragmentation are forced to stop following the evolution soon after the formation of fragments. The time steps required to follow the evolution accurately become prohibitively short due to the decreased dynamic time scale within the high-density fragments. All the computational effort is put into evolving the gas within the fragments, with the result that the calculation effectively grinds to a halt as the low-density gas does not evolve despite the large number of computations being done. This happens regardless of the numerical method used, and despite the use of individual time steps.

When the fragments are formed (and the calculation is halted) they typically contain from $< 1\%$ to 50% of the mass of the original cloud, with the closer multiple systems containing the least amount. This makes it impossible to compare the results of fragmentation calculations with observations, since the final properties of a system depend on the accretion of, or the interaction with, the rest of the cloud material. Indeed, the accretion of the remaining material may even force some 'seed' binaries to merge.

Using SPH, fragmentation calculations may be followed beyond the formation of fragments, if correct internal evolution of the fragments is sacrificed. The important result of a fragmentation calculation is where the material from the cloud ends up - the number of fragments, their masses and orbits. The internal evolution of the fragments is unimportant in the determination of this final state, and thus can essentially be ignored. This allows us to evolve the high-density fragments in a way so as to maintain finite time steps for the particles contained within them, so that the calculation may be followed beyond the formation of the fragments.

One method of following the calculations after the protostellar fragments form is to have a minimum particle smoothing length. For standard fragmentation calculations (although the methods discussed here can be used in any situation where high-density regions are produced), this essentially changes the isothermal equation of state into that of an incompressible gas for the highest-density particles. The separations of the particles no longer decrease and the simulation can be followed longer, at the expense of ignoring the internal evolution of the protostars (e.g. Bonnell et al. 1991). A second method is to change the isothermal equation of state to a polytropic equation of state above a critical density (Bonnell 1994). This is motivated by the fact that, at densities of $10^{-13} - 10^{-14}$ g cm^{-3}, the gas becomes optically thick (see Section 1.1.2). The collapse is no longer isothermal, but instead the gas is heated as it collapses. Following Bonnell (1994), a polytropic equation of state (Equation 2.24) is used, where the polytropic index γ varies with density as

$$\begin{aligned} \gamma = 1.0, \quad \rho \leq 10^{-14} \text{ g cm}^{-3}, \\ \gamma = 1.4, \quad \rho > 10^{-14} \text{ g cm}^{-3}, \end{aligned} \tag{4.1}$$

and the entropy of the gas is kept constant so that the gas has a temperature of 10 K for $\rho \leq 10^{-14}$ g cm^{-3}. This allows the calculations to be followed further as, in heating the gas, the collapse of high-density fragments is slowed. Indeed, with $\gamma = 1.4$ the collapse of a fragment proceeds only as its mass increases, since for a constant mass the thermal energy grows faster than does the magnitude of its gravitational energy (see Equation 1.9). Despite this, however, the additional, unphysical change in γ of

$$\gamma = \tfrac{5}{3}, \quad \rho > 10^{-12} \text{ g cm}^{-3}, \tag{4.2}$$

is also required for the highest-density regions to stop them collapsing under the increasing mass of the accreting fragments. This final change of the equation of state only occurs in the centre of a fragment and is not as visible to particles outside it as when the minimum smoothing length method is used, since the smoothing lengths are still allowed to decrease within the fragment. Hence, the polytropic equation of state provides a more physically correct evolution than the minimum smoothing length method. Both methods maintain finite time steps for particles in fragments, and the calculations can be followed for much longer than with a purely isothermal equation of state.

Calculations done with a minimum smoothing length or a polytropic equation of state are still very computationally expensive, however, and become slower as more particles move to the high-density regions and thus have small time steps. Since the internal evolution of the fragments is not of interest in determining where material from the cloud ends up, a third method can be used. In this method, a fragment is replaced by a single, non-gaseous, massive particle with the combined mass, linear momentum and 'spin' of the particles it replaces. The spin is the angular momentum of the replaced particles about their centre of mass and is kept as a check that global angular momentum is being conserved, although it has no effect on the dynamics of the calculation. This massive particle then accretes any infalling gas particles and avoids the problem of high-density regions controlling the time required for the simulation. This allows a collapsing cloud to be evolved beyond fragment formation to follow the infall of the rest of the cloud's material on to the 'seed' protostellar system. These accreting particles are also used in Chapters 5 and 6 to model protostars in the detailed study of the effects on a 'seed' binary of accretion from a gaseous cloud that remains after the formation of the binary.

The structure of the remainder of this chapter is as follows. Section 4.2 describes the inclusion of non-gaseous, accreting particles in SPH. Three tests of the boundary conditions for the non-gaseous, accreting particles are performed in Section 4.3. Then the evolution of the standard isothermal fragmentation test case proposed by Boss & Bodenheimer (1979) using both standard SPH, and SPH with non-gaseous, accreting particles is presented in Section 4.4 as a test calculation for the particles. Finally, the conclusions are presented in Section 4.5.

4.2 Inclusion of Non-Gaseous, Accreting Particles in SPH

An idea similar to this has been used before (Boss & Black 1982; Boss 1987a, 1989a) to study the collapse of rotating, isothermal interstellar clouds. In these papers, a finite-difference code was used where the central cell was designated as a 'sink cell' which could accrete any infalling gas and its angular momentum. In this way, they were able to study the collapse of clouds beyond the formation of a central protostellar core. These sink cells were fixed in position, however, and therefore accretion on to a binary or multiple protostellar system cannot be studied using this method.

By contrast, the inclusion of dynamic, non-gaseous, accreting particles (sink particles) into SPH is relatively simple, due to the Lagrangian nature of SPH. It involves three main parts. First, the method by which a sink particle accretes infalling gas particles must be decided. Second, a method for the dynamic creation of a sink particle when a protostellar fragment is created during a collapse calculation is required. Finally, boundary conditions between the sink particles and the surrounding SPH gas particles are required.

4.2.1 Accretion By Sink Particles

The sink particle itself is simply a particle, tagged to identify it as a sink particle, with a mass much greater than a typical gas particle (i.e. greater than ≈ 50 times). Sink particles only interact with normal gas particles via gravity (and boundary conditions as is discussed later). Also, gas particles do not interact with other gas particles on the opposite side of a sink particle, except via gravity. Particles that come within a certain radius, the accretion radius r_{acc}, of the sink particle may be accreted. The accretion radius is chosen before the calculation is performed, depending on the resolution required near the sink particle, and remains fixed throughout. All gas particles that come within the accretion radius pass through several criteria to see if they should be accreted. First, the particle must be bound to the sink particle. Second, the specific angular momentum of the particle about the sink particle must be less than that required for it to form a circular orbit at r_{acc} about the sink particle. These conditions ensure particles that would normally leave the accretion radius are not accreted. Finally, the particle must be more tightly bound to the candidate sink particle than to other sink particle. If two sink particles are of unequal mass, it is possible that a particle may briefly pass through the accretion radius of the least massive sink particle, but finally be accreted by the more massive sink particle. This test is included to stop particles being prematurely accreted by the wrong sink particle. Care must also be taken in an individual-time-steps code to ensure that the particle being accreted has just completed a time step.

In addition to the accretion radius described above, a second, inner accretion radius is commonly used. All gas particles coming within this inner radius (which is set to be $10 - 100$ times smaller than the outer accretion radius) are accreted regardless of the tests. This stops particles being accelerated by a close encounter with the sink particle. An alternative is to smooth the potential of the sink particle, as is done in N-body calculations. This inner accretion radius will not be mentioned further.

When a gas particle is accreted, its mass and linear momentum are added to the sink particle. Also, the sink particle's position is shifted to occupy the centre of mass of the gas particle and sink particle. Finally, the spin of the sink particle is modified to take account of the angular momentum about the sink particle that is accreted. The gas particle is then tagged as being accreted, and is no longer involved in the calculation.

4.2.2 Dynamic Creation of Sink Particles

Sink particles can be either included in a simulation from the beginning, or dynamically created during a cloud collapse calculation. The procedure for dynamically creating a sink particle is as follows. When a gas particle in an SPH simulation reaches a specified density (say 10^5 times the initial cloud density), a series of tests are performed to determine if a sink particle should be created from it (see also Price, Bate & Bonnell (1995) for an analytic determination of the density at which testing for sink particle creation should begin, for an isothermal collapse). It is first tested to see if its smoothing length is less than half the accretion radius of the sink particle that will replace it. This is done to ensure that a sink particle is formed from at least ≈ 50 particles (the mean number of neighbours). If this is so, and all the sink particle's neighbours are being evaluated at the current time step (particles are binned into time steps differing by a power of two), then, at the end of this step, the particle and its neighbours undergo a series of tests to decide if they should create a sink particle.

The gas particles should only form a sink particle if they will continue to collapse, if not replaced by a sink particle, rather than expand again. To ensure this, the gas particles must pass four tests. First,

$$\alpha \leq \frac{1}{2}, \tag{4.3}$$

where α is the ratio of thermal energy to the magnitude of the gravitational energy for the particles. Second,

$$\alpha + \beta \leq 1, \tag{4.4}$$

where β is the ratio of rotational energy to the magnitude of the gravitational energy for the particles. Rotation is calculated about the position of the densest particle. Third, the total energy of the particles must be negative. Finally, the divergence of the accelerations on the particles must be less than zero. This final check is done to determine if the particles for the candidate sink particle have a net acceleration away from one another. If they do, the dense region could be in the process of being tidally disrupted or bouncing and should not form a sink particle. In test calculations, sink particle creation almost never fails on this final test alone. If all the tests are passed, a sink particle is formed from the densest gas particle by combining it with its neighbouring gas particles and moving it to the centre of mass.

4.2.3 Boundary Conditions for Sink Particles

Ideally, the introduction of sink particles to an SPH simulation should not affect the evolution of the gas outside the accretion radius. In practice, however, two effects alter the evolution. First, there is some effect because the typically non-spherical, gravitational potential is replaced by a spherical point mass potential, though this should generally be small. Second, and most importantly, there is the discontinuity in the number of particles across the accretion radius due to particles inside being accreted. This affects the pressure and viscous forces on particles outside. Boundary conditions for gas particles near the accretion radius are necessary to correct for this.

Four types of correction to particles near the accretion radius are required. First, the smoothing lengths of particles near the boundary are larger than they would otherwise be, as they are still required to have ≈ 50 neighbours, but they are missing neighbours inside the accretion radius (see Figure 4.1). Second, the density of particles near the boundary is underestimated because the summation in Equation 2.21 is no longer over the entire kernel due to the missing neighbours. Third, particles near the boundary tend to be pushed into the accretion hole because of a lack of pressure forces from the missing particles. Finally, the standard SPH artificial viscosity has bulk viscosity and shear viscosity components (Meglicki, Wickramasinghe & Bicknell 1993). Although in the continuum limit ($h \to 0$) the viscosity present in SPH has no shear viscosity, in a real SPH simulation shear viscosity is present due to the interaction of particles with each other across a shear flow over a finite distance of the order of h. If viscous boundary

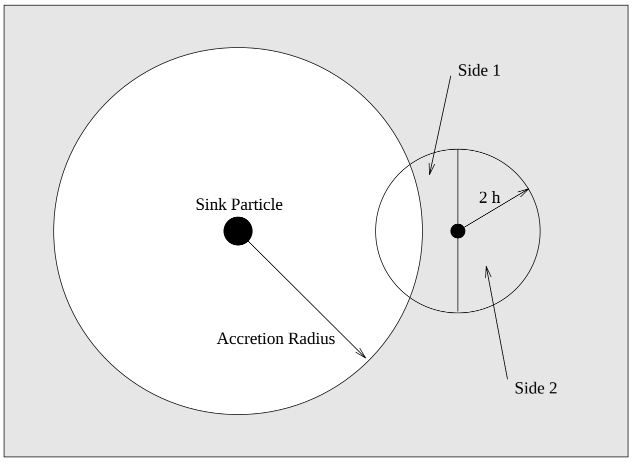

Figure 4.1: The configuration of a typical SPH gas particle near the accretion radius of a sink particle, demonstrating the need for boundary conditions. The volume that contains SPH gas particles is shaded, whereas the inside of the accretion radius contains no gas particles. Hence, the volume of the kernel of a gas particle (of a radius of twice the smoothing length, h) near the boundary has some of its neighbours missing. When the density (or other quantities) is calculated for that particle, the missing neighbours affect the contribution to the density from side 1 of the gas particle, but the contribution from side 2 is unaffected by the accretion hole.

corrections are not made, the lack of neighbours inside the accretion radius can lead to unrealistic angular momentum transport for particles near the boundary via this shear viscosity. For example, in an accretion disc simulation, particles near the boundary are quickly accreted by the sink particle as they lose angular momentum and fall inside the accretion radius (see Section 4.3.3). They still have all of their neighbours further out in the disc which are rotating less rapidly about the sink particle and hence removing angular momentum from them via the shear viscosity. However, they are missing neighbours closer to the sink particle that would have given them angular momentum. Thus, they lose angular momentum much more quickly than is correct, are accreted, and a hole in the disc is rapidly cleared out around the sink particle.

The situations for which boundary conditions around sink particles may be neglected without seriously affecting the calculation are limited. Pressure-related boundary conditions are not required when the radial infall velocity on to the sink particle is supersonic, as this constrains the density and pressure effects to remain near the accretion radius. Viscosity-related boundary conditions are not required when the rotational velocity of the gas around the sink particle is very low compared with the radial infall velocity, or when the dynamics of the simulation change quickly compared with the viscous time-scale of the gas around the sink particle (e.g. due to gravitational torques). In these cases, the effect of the angular momentum transport due to the shear viscosity is small. Note, however, that the viscous time scale is a lot shorter at the boundary than it would be if the medium were continuous, due to the large density gradient across the accretion radius. Examples of cases where boundary conditions are not required are spherical, zero-angular-momentum accretion, and Bondi-Hoyle accretion. Simulations of both these types of accretion have been performed by Price, Bate and Bonnell (1995) using sink particles without boundary conditions. They were found to reproduce one-dimensional, finite-difference code and analytic results well. In most other cases, however, boundary conditions are required.

To avoid the discontinuities at the boundary, we experimented with many different types of boundary condition. One method was to evolve particles, once they had entered the accretion radius, purely under gravity, maintaining constant inward radial velocity, or constant angular momentum, or the rate of angular momentum loss. This method did not provide good viscous boundaries and typically slowed down the calculations by factor of two or three as particles inside the accretion radius were evolved every minimum time step along with the real particles. For the pressure boundary, another attempted method was to add a radial pressure force to particles near the accretion radius from the sink particle by giving the sink particle an effective mass, calculated from its accretion radius and a density extrapolated from its neighbouring particles' densities. This method did not give consistent results for different sized accretion radii.

The final boundary conditions arrived at are as follows. To correct the density and smoothing lengths of particles near the boundary, a linear approximation to the density gradient at each particle's position is found. The neighbours of a particle are sorted by radius from the sink particle and split into two groups. The mean density and radius of these two groups of particles are calculated, allowing a linear fit to the density to be found. The densities from the previous time step are used. This provides an estimate of the radial density gradient at each particle position. In the calculation for a particle's density at the current time step, the contributions to its density in Equation 2.21 from its neighbours on the side facing the sink particle (side 1), and the other side (side 2) are calculated (see Figure 4.1). The former is affected by the accretion hole whereas the latter is not. Half of the self-contribution to the particle's density is also added to contributions from each side of the particle. By integrating the analytic equation for the density,

$$\rho = \int \rho W \; \mathrm{d}^3 r, \tag{4.5}$$

over the volume of the kernel W, assuming a linear density gradient ψ, the expected contribution to the particle's density from each side can be determined. The density is corrected by making the contribution to the density from side 1 of the particle's kernel be the maximum of the SPH summation value and the value given by

$$\rho_1 = \rho_2 \kappa, \tag{4.6}$$

where the subscripts denote sides 1 and 2, and κ is the ratio of the analytic contribution of side 1 to the particle's density to side 2's contribution, assuming the linear density gradient. The ratio κ is given by

$$\kappa = \frac{1-c}{1+c}, \quad \text{where} \quad c = \frac{31 h \psi}{70 \rho} \tag{4.7}$$

when the kernel of Equation 2.20 is used. This ratio is also used to find an approximation to the missing number of neighbours of the particle. Assuming the neighbours are roughly equally spaced on both sides, κ gives the ratio of the numbers of neighbours on each side of the particle, allowing the number of missing neighbours to be determined. This extra number of missing neighbours is taken into account when altering the particle's smoothing length.

For the pressure correction, only radial pressure accelerations on boundary particles are corrected. Using the same method as is used to determine the density gradient, an approximation to the pressure gradient at a particle's position is determined. Then using

$$\frac{\mathrm{d}v_{\mathrm{p}}}{\mathrm{d}t} = -\frac{1}{\rho}\frac{\mathrm{d}P}{\mathrm{d}r} \tag{4.8}$$

the expected radial acceleration due to pressure on the particle is found. This is compared with the radial pressure acceleration on the particle as determined by the SPH summation equations. If the expected value gives a greater outward acceleration than the SPH value, a radial acceleration correction, which is the difference of the expected and SPH values, is added to the particle's acceleration. To conserve linear momentum, an equal and opposite force is applied to the sink particle.

Boundary conditions for the artificial viscosity forces are not as simple as the other corrections. With shear viscosity, forces can be given to a particle from shear flows in several directions. Also, the magnitude of the force depends on the second derivative of the velocity across the shear flow, and on the density gradient. In addition, viscous forces on particles can be given by shocks as well as shear flow. Analytic corrections become very complicated.

Instead, a simpler method is used. First, the direction of the smoothed velocity is calculated for each particle near the boundary and for all their neighbours. This is calculated by summing the particle's velocity and all its neighbours' velocities, weighted by the kernel. Then, for each particle, the components of these smoothed velocities that are orthogonal to the radial vector to the sink particle are found. Using these velocities, the component of the viscous acceleration on a particle that is directed tangentially to the accretion hole, and in the direction of motion of the particle, is found for each particle using the corrected viscous accelerations from the previous time step. Once this component of the viscous acceleration has been calculated for each particle, an estimate of the correct viscous acceleration on a particle in this direction is calculated as the mean of these values for each of the particle's neighbours that are further in radius from the sink particle than the particle itself. Using the estimate of the viscous tangential acceleration in this direction, a correction is added to the particle's viscous acceleration in a similar way to the radial pressure acceleration correction. The value of the correction is the difference between the estimated viscous tangential acceleration and the SPH value calculated at the current time step in this direction, with the constraint that the net viscous acceleration on the particle cannot be in its direction of motion to avoid giving particles extra angular momentum (i.e. particles near the boundary can be stopped from losing angular momentum, but cannot gain angular momentum). Again, to conserve linear momentum an equal and opposite force is applied to the sink particle, and in this case a correction to the sink particle's spin is also made to conserve angular momentum. If the constraint that a particle near the boundary cannot increase its angular momentum is not included, two effects can lead to incorrect results. First, a runaway situation is possible. The particle may interact with its neighbours that are further from the sink particle, giving them accelerations in their direction of motion, in turn increasing the acceleration given to the boundary particle. Second, the correction is intended to handle the shear viscosity discontinuity at the boundary, but viscous accelerations can also be given by shocks, which may not be estimated well. Since the angular momentum for the correction comes from the sink particle's spin there is, potentially, an unlimited source of angular momentum for these two effects to inject into the surrounding gas. Hence, allowing angular-momentum-increasing viscous accelerations can lead to incorrect results and they should not be allowed.

Viscous accelerations on particles near the boundary that are directed radially, and viscous accelerations directed orthogonally to the direction of motion of the particle and the radial direction, are not altered even though they are also affected by the presence of the accretion hole. However, since the action of viscosity is to resist motion, and viscous accelerations in the direction of motion of the particles and orthogonal to the radial direction are corrected, the major boundary effect is corrected. To attempt to correct the viscous forces in the other directions by this method could be worse than having no correction at all, due to the presence of shocks.

Finally, the boundary conditions for a particle are applied gradually as the sink particle is approached. This is achieved by multiplying the corrections by a smoothly varying function χ ranging between zero and unity as the particle approaches the sink particle. The functional form of χ is relatively unimportant and for simplicity the un-normalised kernel function

$$\chi = \begin{cases} 1 & \text{if } x < 0, \\ \pi h^3 W(x,h) & \text{if } 0 \le x \le 2, \\ 0 & \text{if } x > 2, \end{cases} \tag{4.9}$$

is used, where $x = 2(r - r_{\rm acc} - h)/h$ for the corrections to the density and number of neighbouring particles, and $x = 4(r - r_{\rm acc} - 3h/2)/h$ for the corrections to pressure and viscous forces. The different forms of x reflect the radii at which neighbouring particles have a large contribution to the calculation of a particle's density and the pressure and viscous forces upon it. In addition, if a particle is a neighbour of two or more sink particles, then no boundary corrections are applied to it.

A comparison of the quantities near the edge of an accretion radius between calculations with and without boundary conditions is shown in Figure 4.2. The simulation has been created by placing a sink particle at the centre of an already-formed disc. The difference made by including boundary conditions is readily apparent. The smoothing lengths of particles near the boundaries no longer increase due to a lack of neighbours. The density does not drop off, but continues to increase toward the centre. The radial

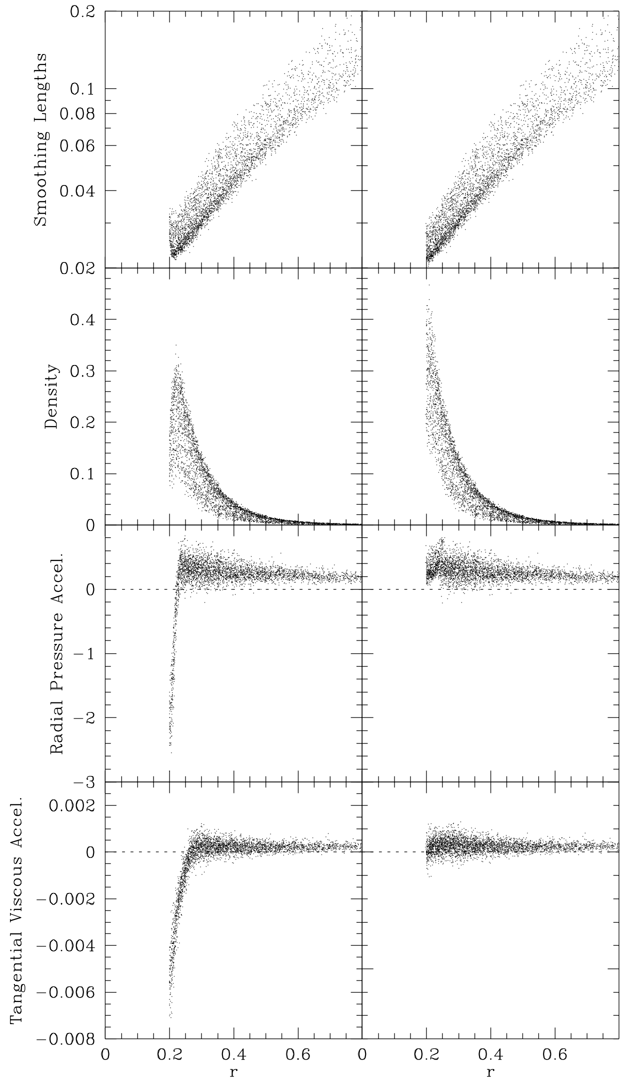

Figure 4.2: The smoothing lengths (top), densities (upper middle), radial pressure accelerations (lower middle), and mean viscous accelerations in the direction of motion (bottom) of particles in a disc surrounding a sink particle. These are shown without (left) and with (right) boundary conditions at the accretion radius. The units are arbitrary with the gravitational constant $G = 1$.

pressure accelerations on particles near the boundary are no longer inward, but are corrected to have net outward accelerations due to pressure. Finally, the mean of the viscous tangential accelerations (calculated for each particle from the viscous tangential accelerations on a particle and all its neighbours) are now approximately zero, rather than being negative, which would cause the particles to fall inside and be accreted. The mean over a particle and its neighbours is plotted rather than the actual viscous accelerations as, at any one moment, these tend to be very noisy. As previously mentioned, individual particles with boundary corrections are not allowed angular-momentum-increasing accelerations. This gives the slight drop of the mean viscous tangential accelerations in Figure 4.2 toward the boundary and results in a slightly higher accretion rate of particles than if the full correction was used. Tangential viscous accelerations that give net angular momentum to a particle near the boundary can be allowed in a stable disc simulation, although, if shocks and other instabilities are present, it is safest not to allow angular-momentum-increasing corrections to be applied to particles.

4.3 Tests of Sink Particle Boundary Conditions

The boundary conditions have already been shown to correct the density, pressure, viscous forces and number of neighbours of particles near the accretion radius of a sink particle in an axisymmetric disc (Figure 4.2). Here the boundaries are tested in dynamic simulations. First, spherical accretion is tested, with the results compared to a one-dimensional, Lagrangian, finite-difference code. Second, Bondi-Hoyle accretion calculations are performed and the results are compared to the expected accretion rates. Finally, the formation of a gas disc around a sink particle is studied.

4.3.1 Spherical Accretion

Calculations of zero-angular-momentum, spherical, gaseous accretion on to a point mass, modelled by a sink particle, have been performed by Price, Bate and Bonnell (1995). They show that sink particles without boundary conditions model the accretion flow well. Boundary conditions are not required to obtain the correct accretion rates for two reasons. First, unless $r_{\rm acc}$ is very large, the flow across the accretion radius is supersonic; pressure effects near the accretion radius cannot propagate outward to affect the infall of material upstream. Second, the flow is purely radial so there is no transport of angular momentum via viscous torques and thus corrections to the artificial viscosity are not required. In this section, the boundary conditions given in Section 4.2.3 are tested to check that they do not disrupt spherical accretion on to a point mass.

The test calculation consists of the isothermal collapse of an initially uniform-density, non-rotating cloud of molecular hydrogen. The cloud initially has mass $M = 1.0$ M$_\odot$, radius $R = 1.15 \times 10^{17}$ cm, and $T = 10$ K. This gives a ratio of thermal energy to the magnitude of gravitational energy of $\alpha = 0.90$. Due to the isothermal equation of state, the cloud collapses to form a high-density core. The rest of the cloud then falls on to the core over several initial cloud free-fall times ($t_{\rm ff} = 3.76 \times 10^{12}$ s). The high-density core is modelled in the SPH calculations by a sink particle. Constant-volume boundary conditions are employed at the outer boundary of the cloud.

The SPH calculations use ≈ 15000 particles. For comparison, the collapse is also followed with a one-dimensional, finite-difference code (see Section 3.4). The finite-difference code uses a sink cell at the centre of the calculation of less than 0.3% of the cloud radius. Sink particles/cells are formed when the central density of the cloud reaches 10^5 times the initial density. By comparing the sink particle and sink cell formation times, it is found that the SPH calculations take 17% longer than the finite-difference code to form a sink particle. The initial cloud is very close to being stable against collapse, and

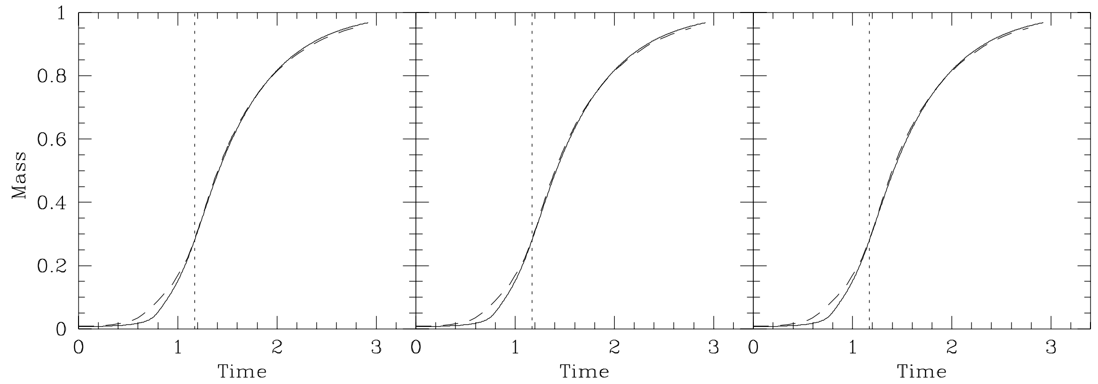

Figure 4.3: The mass contained within a radius of 1/5 of the initial cloud radius R during the collapse of an initially uniform-density, non-rotating cloud with various types of SPH sink particle (dashed lines). The sink particles have accretion radii: $r_{\rm acc} = R/50$ with boundary conditions (left); $r_{\rm acc} = R/5$ without boundary conditions (centre), $r_{\rm acc} = R/5$ with boundary conditions (right). Each case is compared to results from a one-dimensional, finite-difference code (solid line). The vertical line gives the time at which a sink particle or sink cell is created in the calculations. Mass is measured in $M_\odot$, and time in units of the initial cloud free-fall time $t_{\rm ff} = 3.76 \times 10^{12}$ s.

therefore any additional energy that is pumped into the calculation noticeably delays the collapse. With SPH this energy can arise from the boundary conditions at the outer edge of the cloud - ghost particle boundaries are used. Thus, the longer collapse time taken for the SPH calculations is not unexpected. To allow comparison between the SPH and finite-difference codes, the SPH time has been shifted so that sink particle formation coincides with sink cell formation using the finite-difference code.

Figure 4.3 gives the mass contained within $r = R/5$ of the sink particle as a function of time for various SPH calculations, along with the finite-difference code comparison. Early on, before a sink particle/cell is created, the calculations performed with SPH contain slightly more mass in the centre of the cloud than with the finite-difference code. This is presumably the result of the energy being pumped into the cloud from the outer boundary. Despite this, the finite-difference and SPH codes give nearly identical results once the collapse becomes supersonic. In particular, all the SPH calculations are in good agreement with the finite-difference code, and with each other, after the sink particle/cell is created. The results are the same regardless of whether a small or large accretion radius is used and regardless of whether sink particle boundary conditions are used or not. Figure 4.4 shows the density and velocity as a function of radius for various SPH calculations, along with the finite-difference code, at $t = 0.05t_{\rm ff}$ after the formation of a sink particle/cell. For the SPH calculation performed without boundary conditions, the radial-infall velocity is too large near the accretion radius due to the absence of pressure forces on particles from within the accretion radius. The density is also underestimated near the accretion radius. With boundary conditions for the sink

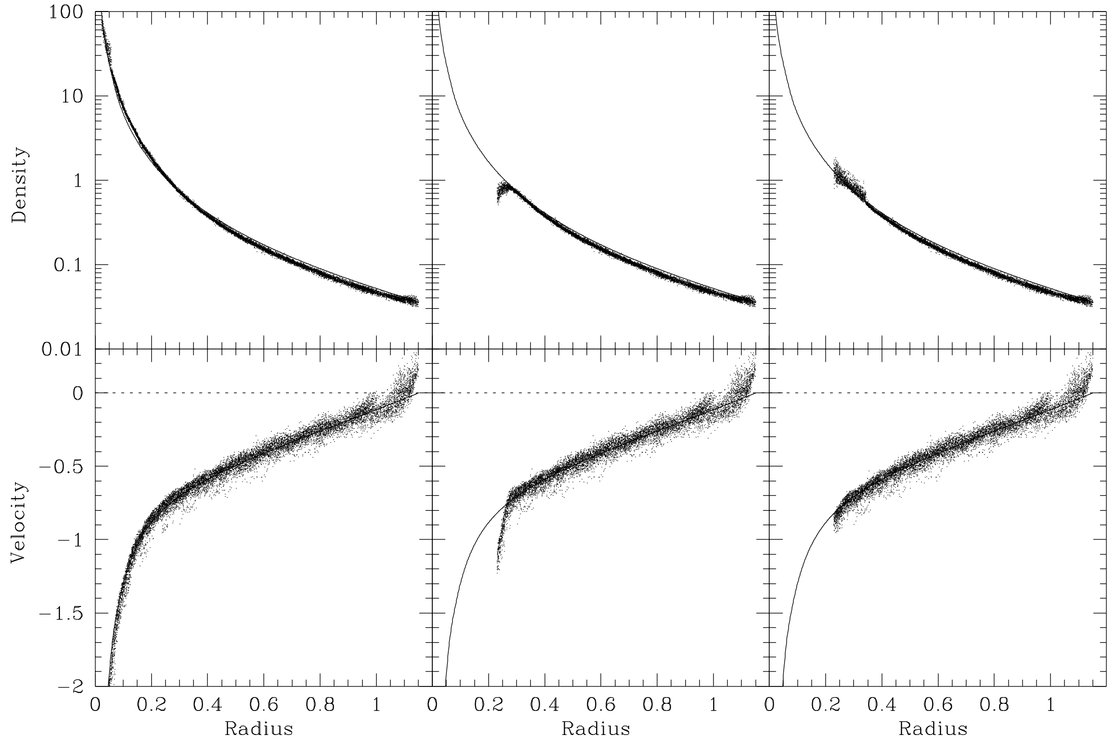

Figure 4.4: Density (top) and velocity (bottom) as a function of radius for the collapse of an initially uniform-density, non-rotating cloud with various types of SPH sink particle. The sink particles have accretion radii: $r_{\rm acc} = R/50$ with boundary conditions (left); $r_{\rm acc} = R/5$ without boundary conditions (centre), $r_{\rm acc} = R/5$ with boundary conditions (right). In each case, comparison is made with a one-dimensional, finite-difference code (solid line). The units are given by using $G = 1$ with mass measured in $\rm M_\odot$ and distance in units of 10^{17} cm.

particle, the velocity and density profiles match the finite-difference code and small-accretion-radius SPH results much better.

Therefore, as expected, boundary conditions are not required to give the correct spherical accretion rate on to the point mass since the flow at the accretion radius is supersonic. Calculations both with and without boundary conditions give the correct accretion rates. Boundary conditions do, however, correct the local properties of the gas near the accretion radius.

4.3.2 Bondi-Hoyle Accretion

Bondi-Hoyle accretion calculations were also performed by Price, Bate and Bonnell (1995) with SPH using sink particles without boundary conditions. As with spherical accretion, sink particles without boundary conditions were found to give the expected accretion rate on to the sink particle. This was result was independent of the accretion radius of the sink particle, although only accretion radii less than the Bondi-Hoyle accretion radius were used. The results of Bondi-Hoyle accretion calculations performed using sink particles with boundary conditions are now presented.

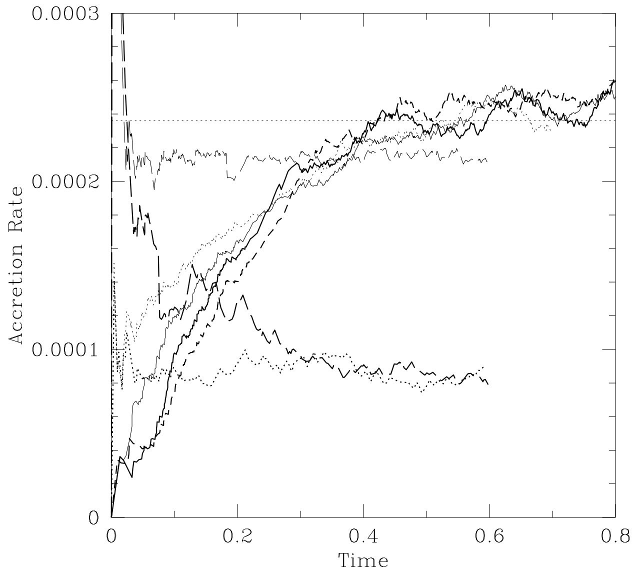

Figure 4.5: The accretion rates as functions of time for point masses (modelled by sink particles) passing at Mach 3 through a uniform-density column of gas. In all cases, a steady-state accretion flow is quickly attained, but for large-accretion-radii sink particles the accretion rates are too low. The sink particles are used with (thick lines) and without (thin lines) boundary conditions. The sink particles have accretion radii of $r_{\rm acc} = 0.02$ (solid), $r_{\rm acc} = 0.04$ (short-dashed), $r_{\rm acc} = 0.08$ (dotted), $r_{\rm acc} = 0.16$ (long-dashed). In the units used here ($M = 1$, $G = 1$, $c_\infty = 1$, $\rho_\infty = 1/(600\pi)$), the expected Bondi-Hoyle accretion rate is $\dot{M}_{\rm BH} = 0.000236$ with $\lambda = \lambda_{\rm c}$ (horizontal line). The effective cross section for the accretion is $R_{\rm BHL} = 0.22$.

For spherical accretion on to a stationary point mass from a uniform-density, gaseous medium, the accretion rate is given by

$$\dot{M}_{\rm sp} = \lambda\ 4\pi\rho_\infty \frac{(GM)^2}{c_\infty^3}, \tag{4.10}$$

where M is the mass of the accretor, and c_∞ and ρ_∞ are the sound speed and density, respectively, of the unperturbed gas an infinite distance from the accretor. The parameter λ is dependent on the equation of state of the gas. For isothermal gas, the value of λ is a maximum and is equal to

$$\lambda_{\rm c} = \frac{1}{4} e^{3/2} = 1.1204... \tag{4.11}$$

The accretion rate on to a point mass moving at a speed v_∞ through a pressure-less medium (i.e. $c_\infty \ll v_\infty$ so that the gas is non-interacting except along the downstream axis where the streams collide) is given by (Hoyle & Lyttleton 1939, 1940a, b, c)

$$\dot{M}_{\rm HL} = \pi R_{\rm BHL}^2 \rho_\infty v_\infty, \tag{4.12}$$

where the effective cross section for the accretion $R_{\rm BHL}$, is given by the Bondi-Hoyle-Lyttleton accretion radius

$$R_{\rm BHL} = \frac{2GM}{v_\infty^2}. \tag{4.13}$$

Boundary Conditions	r_{acc}	Accretion Rate
No	0.02	0.000246 ± 0.000015
	0.04	0.000239 ± 0.000013
	0.16	0.000215 ± 0.000014
Yes	0.02	0.000242 ± 0.000015
	0.04	0.000246 ± 0.000014
	0.08	0.000087 ± 0.000010
	0.16	0.000085 ± 0.000010

Table 4.1: The accretion rates for the various Bondi-Hoyle accretion calculations performed with SPH and sink particles. In the units used here ($M = 1$, $G = 1$, $c_\infty = 1$, $\rho_\infty = 1/(600\pi)$), the expected accretion rate is $\dot{M}_{\mathrm{BH}} = 0.000236$ with $\lambda = \lambda_{\mathrm{c}}$.

In general, accretion on to a moving point mass is known as Bondi-Hoyle accretion and the accretion rate lies somewhere between the above two limits. Bondi and Hoyle (1944) and Bondi (1952) suggested a formula for interpolating between the zero-velocity and high-velocity limits. This was corrected and compared to numerical calculations (Dodd 1952, 1953; Dodd & McCrea 1952; McCrea 1955; Hunt 1971, 1979; Shima et al. 1985; Ruffert & Arnett 1994) to give a general accretion rate of

$$\dot{M}_{\mathrm{BH}} = \lambda_* 4\pi \rho_\infty \frac{(GM)^2}{(v_\infty^2 + c_\infty^2)^{3/2}}, \tag{4.14}$$

where $\lambda_* = \lambda$ for $v_\infty = 0$, and $\lambda_* \rightarrow 1$ as $v_\infty \rightarrow \infty$. The flow has Mach number $\mathcal{M}_\infty = v_\infty / c_\infty$.

We now present the results of several Bondi-Hoyle accretion calculations performed with SPH and sink particles. The simulations are performed by passing a point mass down a cylindrical column of uniform-density, isothermal gas. The point mass is modelled by a sink particle, and the gas by 30000 particles randomly distributed within the column. The total mass of the gas is 1/100 the mass of the point mass and the gas is non-self-gravitating. Ghost particles are created at the outer boundary of the cylinder to contain the gas. The sink particle passes through the column of gas, and the accretion rate is calculated once a steady accretion flow has been obtained. It is found that the dimensions of the cylinder must be large enough so that a sound wave cannot propagate from the outer boundary of the cylinder into its centre during during the calculation. If this is not satisfied, the accretion rate is affected and does not attain a steady flow. In all calculations $\mathcal{M}_\infty = 3$.

The accretion rates of the Bondi-Hoyle accretion simulations as a function of time are given in Figure 4.5, along with the expected accretion rate given by Equation 4.14 with $\lambda = \lambda_{\mathrm{c}}$. Results are given for calculations performed with and without boundary conditions, and with different values of the sink particle's accretion radius. In each case, the rate of change of mass of the sink particles with time over the period of steady accretion is given in Table 4.1. The SPH results agree best with the value of the accretion rate given using $\lambda = \lambda_{\mathrm{c}}$ for small-accretion-radii calculations. All calculations without

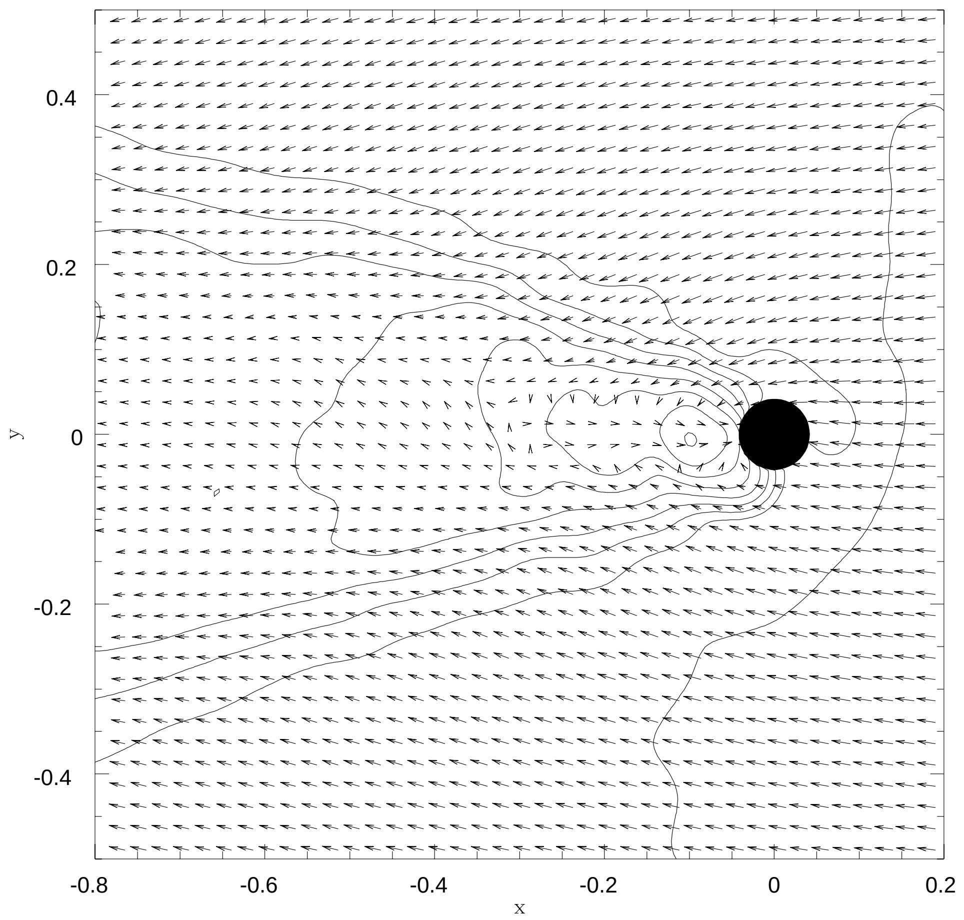

Figure 4.6: The gas density and velocity field around a point mass passing at Mach 3 through a gaseous medium. Velocity is shown in the frame of the point mass. The point mass is modelled by a sink particle with boundary conditions and an accretion radius of $r_{\rm acc} = 0.04$ (the size of the filled circle). A Bondi-Hoyle accretion trail behind the point mass is observed. The density contours are in levels of 0.2 decades, and the length of the arrows is proportional to the speed of the flow. The effective cross section for the accretion is $R_{\rm BHL} = 0.22$.

sink particle boundary conditions give almost the same accretion rate, even with $r_{\rm acc} \approx 0.7 R_{\rm BHL}$.

When boundary conditions are included around the sink particle, the correct accretion rate is given provided

$$3h_{\rm acc} \lesssim (R_{\rm BHL} - r_{\rm acc}), \tag{4.15}$$

where $h_{\rm acc}$ is the smoothing length of particles near the accretion radius. If $h_{\rm acc}$ is larger than this, the accretion rate is lower than expected. In Bondi-Hoyle accretion, particles swing past the point mass, collide behind it, fall toward the point mass, and are accreted. If the smoothing lengths are too large, the viscous accelerations required to stop the particles in the colliding streams are lost when the boundary conditions are applied, and the shock behind the point mass is not resolved. The viscous accelerations on particles

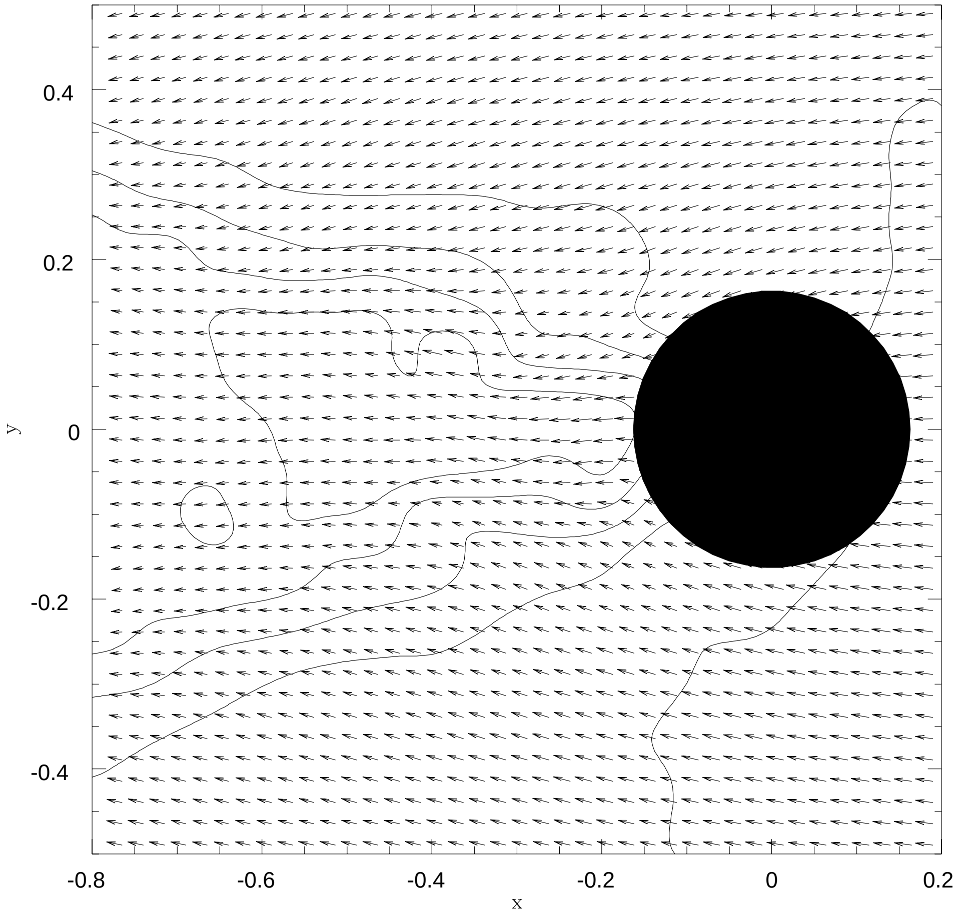

Figure 4.7: The gas density and velocity field around a point mass passing at Mach 3 through a gaseous medium. Velocity is shown in the frame of the point mass. The point mass is modelled by a sink particle with boundary conditions and an accretion radius of $r_{\rm acc} = 0.16$ (the size of the filled circle). The flow near the point mass is not well modelled, and a Bondi-Hoyle accretion trail is not observed. The density contours are in levels of 0.2 decades, and the length of the arrows is proportional to the speed of the flow. The effective cross section for the accretion is $R_{\rm BHL} = 0.22$.

near the accretion radius are estimated to be the mean of the viscous accelerations on particles farther out. This estimate is applied to particles according to Equation 4.9, and so has an affect on viscous forces out to $r_{\rm affect} = r_{\rm acc} + 2h_{\rm acc}$. An additional smoothing length more than this is required to give the correct viscous forces outside $r_{\rm affect}$ from which the estimated forces within $r_{\rm affect}$ are calculated, and hence Equation 4.15 is required for the accretion trail to be resolved.

If Equation 4.15 is not satisfied, particles that pass behind the point mass dissipate less energy than they should, and too few particles are accreted. This is apparent when the density and velocity of the Bondi-Hoyle accretion flow is considered (Figures 4.6 and 4.7). For a small-accretion-radius calculation (Figure 4.6), the accretion trail behind the point mass is well resolved. When a large accretion radius is used with boundary conditions, the accretion flow is disrupted and an accretion trail is not formed behind the point mass (Figure 4.7). Instead of the streams colliding behind the point mass, dissipating their kinetic energy, and falling on to the point mass, the gas retains enough kinetic energy to escape the point mass and the accretion rate is reduced. Note that only the viscous boundary conditions, and not the other three corrections, cause this disruption to Bondi-Hoyle accretion. This effect must be considered when setting the accretion radius. Alternately, it may be possible to implement a switch, employing viscous boundary conditions only when the net rotation of the gas around the sink particle is significant. For example, for a sink particle surrounded by an accretion disc viscous boundary conditions would be used, but they would not be used for Bondi-Hoyle or spherical accretion.

4.3.3 Disc Formation Around a Sink Particle

To demonstrate the effectiveness of the sink particle boundaries when rotational support is important near a sink particle, results are presented from a calculation of the non-self-gravitating collapse of a spherical, rotating, uniform-density cloud to form a disc around a sink particle. The initial conditions consist of a spherical, uniform cloud of molecular hydrogen in solid-body rotation with mass M, radius R, temperature T, and rotational frequency Ω, of

$$\begin{array}{ll} M = 0.001\ \mathrm{M}_\odot, & R = 2.56 \times 10^{16}\ \mathrm{cm}, \\ T = 10\ \mathrm{K}, & \Omega = 1.54 \times 10^{-12}\ \mathrm{rad\ s^{-1}}, \end{array} \tag{4.16}$$

surrounding a 1 $\mathrm{M}_\odot$ star at the centre of the cloud, which is represented by a sink particle. The cloud collapses isothermally, under the gravity of the central sink particle only, to form a non-self-gravitating disc around the sink particle. The calculation is performed with two different accretion radii. If the use of sink particles affects the dynamics of the gas outside the accretion radius, the mass contained within a given radius at any one moment will be different for simulations using different accretion radii.

Figure 4.8 shows the formation of the disc around the sink particle for four different calculations. The first two are performed with no boundary conditions at the accretion radius of the sink particle, and have $r_{\rm acc} = 0.01$ and $r_{\rm acc} = 0.05$ in units of 10^{16} cm. In both cases, the central region of the disc is cleared out to a radius much larger than the accretion radius, mainly due to the lack of a viscous boundary condition. When boundary conditions are added to the sink particle implementation, the situation is vastly improved. The early formation of the disc is much better handled, and later in the calculation the central regions of the discs are no longer cleared out due to the discontinuity. Instead, particles are present right up to the accretion radius. Near the end of the calculation, particles are still deficient at the centre of the disc, especially in the small accretion radius case. However, most of this is not due to the lack of a boundary condition. To understand this effect, we must consider how the mass contained within $r = 0.05$ of the sink particle changes with time. This is shown in Figure 4.9. For the two

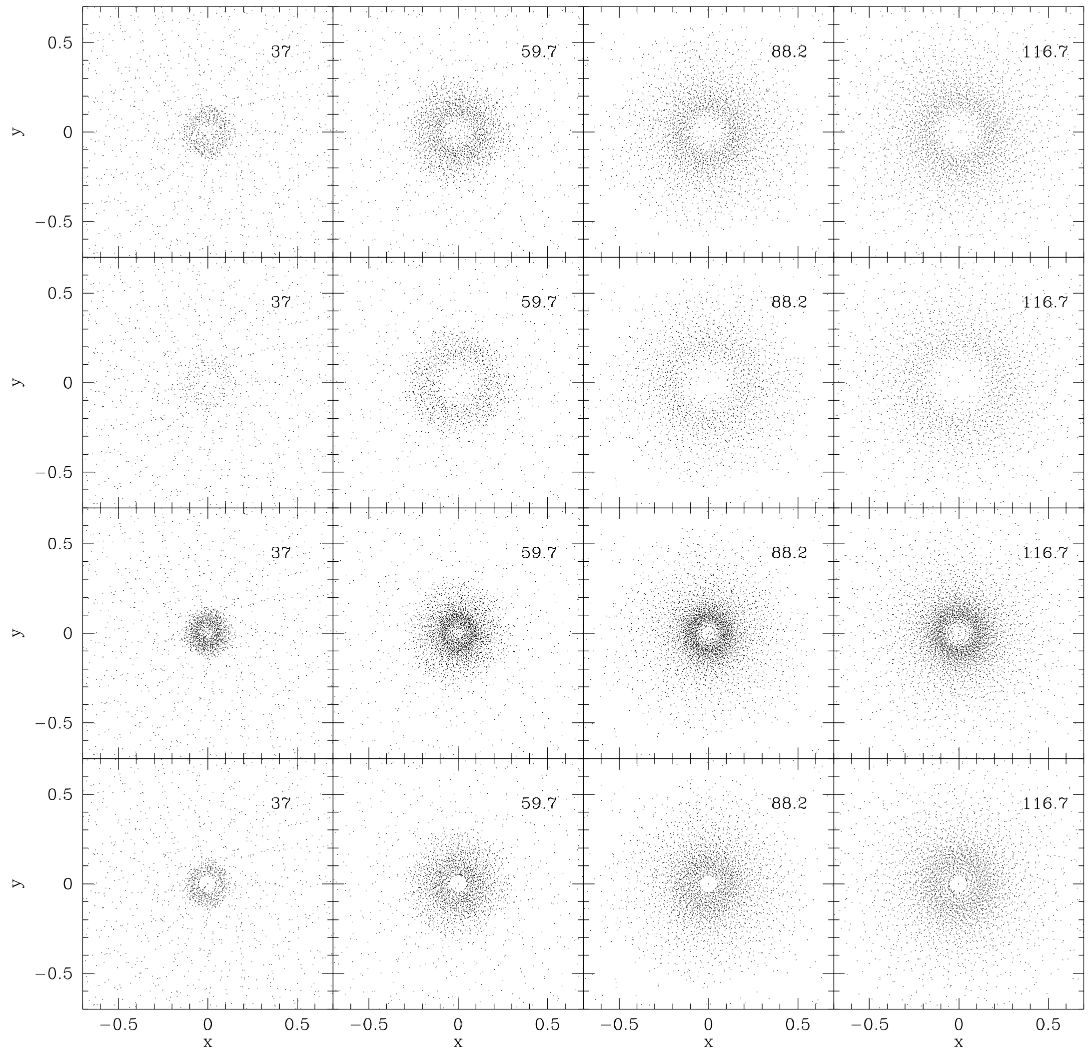

Figure 4.8: The formation of a disc around a sink particle for four different cases. The first two cases have no boundary conditions at the accretion radius $r_{\rm acc}$, of the sink particle and have $r_{\rm acc} = 0.01$ (top) and $r_{\rm acc} = 0.05$(upper middle). The second two cases are performed with boundary conditions at the accretion radius of the sink particle and again have $r_{\rm acc} = 0.01$ (lower middle) and $r_{\rm acc} = 0.05$ (bottom). The boundary conditions stop the excess accretion from the disc that occurs in calculations without boundary conditions due to the accretion hole. The calculation is performed with 5000 particles. The time, in units of the orbital period of a particle at $r = 0.05$, is given in the upper right-hand corner of each panel. The axes are in units of 1.0×10^{16} cm.

calculations without boundary conditions, the rate at which material enters $r = 0.05$ is larger with the larger accretion radius than with the smaller-accretion-radius as the disc is formed. However, later on both calculations have the same growth rate of mass within $r = 0.05$. As is shown in Figure 4.8, this is because the central regions of the disc are cleared out in both cases, faster initially with the larger accretion radius, but later both discs are cleared out to much greater than $r = 0.05$ and the accretion then

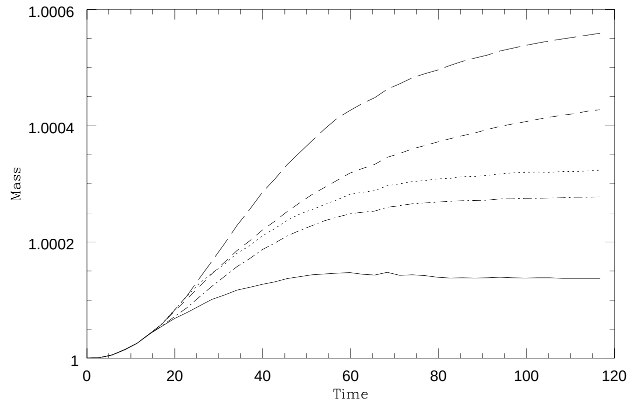

Figure 4.9: The formation of a disc around a sink particle, showing how the mass contained within $r = 0.05 \times 10^{16}$ cm of the sink particle (including the sink particle's original mass) increases with time. The results for an accretion radius of $r_{\rm acc} = 0.01 \times 10^{16}$ cm are shown with (solid) and without (short-dashed) boundary conditions. Calculations with $r_{\rm acc} = 0.05 \times 10^{16}$ cm are also shown with (dotted) and without (long-dashed) boundary conditions. Finally, the mass that has been inside $r = 0.05 \times 10^{16}$ cm at any time during the calculation with $r_{\rm acc} = 0.01 \times 10^{16}$ cm is shown for the case with boundary conditions (dot-dashed). The calculation was performed with 5000 particles. Mass is given in $M_\odot$, and the time is in the units of the orbital period of a particle at $r = 0.05 \times 10^{16}$.

depends on the flow of mass through the accretion disc, which is similar for both cases. When boundary conditions are included in the calculations, the masses contained within $r = 0.05$ of the sink particle differ even more, with less mass being contained by the smaller accretion radius calculation. However, the amount of material that has been within $r = 0.05$ of the sink particle, at some point during the calculation, is largely independent of accretion radius. This demonstrates that the boundary conditions of the sink particle are working well. The reason that the mass contained within $r = 0.05$ of the small-accretion-radius sink particle at a specific time is less than the mass that has been within this radius at any time during the calculation is that the evolution inside the radius is such that the outer material gains angular momentum from material further in due to shear viscosity and so moves out of the $r = 0.05$ region. This can be seen in the way in which the mass within $r = 0.05$ for the small accretion radius calculation decreases with time after the disc has formed. The deficiency of particles in the inner parts of the discs at late times seen in Figure 4.8 is now explained. The boundary conditions are behaving well, but outward evolution of mass from the inner parts of the disc cannot be followed correctly since material that has been accreted cannot re-enter the simulation. Particles that would have evolved outward into the deficient zone were accreted earlier by the sink particle. A difference between the mass within $r = 0.05$ at a specific time and the mass that has been within this radius at any time did not occur in the small-accretion-radius calculation without boundary conditions, as accretion due to the lack of boundary conditions overwhelmed the gain in angular momentum from the material inside $r = 0.05$.

The transport outward also explains most of the difference between the large-accretion-radius and small-accretion-radius calculations when considering the mass that has been within $r = 0.05$ at some point during the calculation. When the disc is forming, the smaller accretion radius calculation transfers some angular momentum from inside $r = 0.05$ to outside via viscosity, allowing less material to enter the $r = 0.05$ region. This cannot occur with the large-accretion-radius calculation as there are no particles inside $r = 0.05$ and angular-momentum-increasing accelerations on particles near the boundary are specifically not allowed by the boundary conditions. Later, when the disc has fully formed, material enters $r = 0.05$ only slightly faster with the large accretion radius than with the small accretion radius. Again this is because angular-momentum-increasing accelerations are not allowed by the boundary conditions. Although the mean tangential accelerations on the particles near the boundary are nearly zero once the disc has formed, numerical noise means that some particles have negative and some positive accelerations, and, since positive accelerations are not allowed, the mean is slightly negative giving a slightly increased accretion rate. If angular-momentum-increasing accelerations are allowed by the boundary conditions, the small and large accretion radius calculations give more similar results. This is possible in a stable disc calculation, but, as was explained earlier, is not advisable generally. Despite this constraint, however, the boundary conditions give a vast improvement over the case without boundary conditions.

4.4 Standard Isothermal Test Case

We now demonstrate the promise of incorporating sink particles in SPH to allow the evolution of cloud fragmentation calculations beyond protostellar creation, and thus determine the final system states. The chosen example is the standard isothermal test case for the fragmentation of a molecular cloud. This was first described by Boss & Bodenheimer (1979), and since then has become a typical test case for numerical codes studying fragmentation processes (Bodenheimer, Tohline & Black 1980; Bodenheimer & Boss 1981; Monaghan & Lattanzio 1986; Boss 1986; Myhill & Boss 1993). The initial conditions consist of an isothermal, spherical cloud of molecular hydrogen gas. The cloud's mass M, radius R, temperature T, and rotational frequency Ω are

$$\begin{aligned} M &= 1.0\ \mathrm{M}_\odot, & R &= 3.2\times10^{16}\ \mathrm{cm}, \\ T &= 10\ \mathrm{K}, & \Omega &= 1.56\times10^{-12}\ \mathrm{rad\ s^{-1}}, \end{aligned} \tag{4.17}$$

resulting in ratios of thermal energy to the magnitude of gravitational energy, and rotational energy to the magnitude of gravitational energy of $\alpha = 0.25$ and $\beta = 0.20$, respectively. Note that a value of Ω slightly less than the value of 1.6×10^{-12} rad s^{-1} that is usually quoted is used, as this gives β closer to 0.20. In addition, there is an $m = 2$ density perturbation imposed on the cloud depending only on the azimuthal angle ϕ, given by

$$\rho = \rho_0[1 + 0.5\ \sin(2\phi)] \tag{4.18}$$

Fragment Properties	Isothermal	Polytropic	M64	B64
$M_{\mathrm{f}}/\mathrm{M}_{\odot}$	0.17	0.17	0.15	0.10
α_{f}	0.02	0.10	0.08	0.13
β_{f}	0.24	0.28	0.29	0.38
$(J/M)_{\mathrm{i}}/(J/M)_{\mathrm{f}}$	12	12	10	12
D/R	0.29	0.29	0.28	0.32

Table 4.2: Fragment properties from the Boss & Bodenheimer (1979) standard test case performed with SPH at 1.32 initial cloud free-fall times. Columns M64 and B64 give the results of Myhill & Boss (1993) for comparison.

where $\rho_0 = 1.44 \times 10^{-17}$ g cm^{-3}. The initial cloud free-fall time is $t_{\mathrm{ff}} = 5.52 \times 10^{11}$ s.

Previous calculations of the standard test case have shown that the cloud forms two fragments due to the $m = 2$ density perturbation. Until now the fragmentation of this test case has not been followed beyond 1.9 free-fall times (Monaghan & Lattanzio 1986), and commonly is only evolved until about 1.3 free-fall times (Boss & Bodenheimer 1979; Bodenheimer, Tohline & Black 1980; Bodenheimer & Boss 1981; Boss 1986; Myhill & Boss 1993). This is not long enough even to determine if the binary fragmentation survives, or merges as the two fragments fall toward each other. Indeed, it has been speculated that the fragments merge, and do not form a binary system (Monaghan & Lattanzio 1986).

4.4.1 Standard SPH Fragmentation

To test how the evolution of a fragmentation calculation is affected by the use of sink particles, the calculation must first be evolved without sink particles. With a purely isothermal equation of state, the calculations are forced to halt at 1.27 initial cloud free-fall times t_{ff} due to the high densities reached. However, the introduction of a minimum particle smoothing length or a polytropic equation of state allows the standard test case to be evolved further. In two calculations, the standard test case was evolved with standard SPH to 2.2 t_{ff}. One simulation maintained finite time steps via a minimum particle smoothing length, keeping the gas isothermal. The minimum smoothing length was set to be 1% of the initial cloud radius. The other simulation used the polytropic equation of state described in Section 4.1 and no minimum smoothing length. Figure 4.10 shows the fragmentation as calculated with the polytropic equation of state. The initial evolution is almost identical in both cases. The cloud initially forms two fragments that collapse on themselves. The fragmentation does not proceed via the initial formation of a bar structure, as seen in early calculations (Bodenheimer & Boss 1981). Instead, the two fragments are distinct from the beginning of their formation. This agrees with the later finite-difference code results (Myhill & Boss 1993).

To allow comparison of the SPH results with the results of Myhill & Boss (1993), the initial fragment properties are listed in Table 4.2 for both simulations at 1.32 t_{ff}.

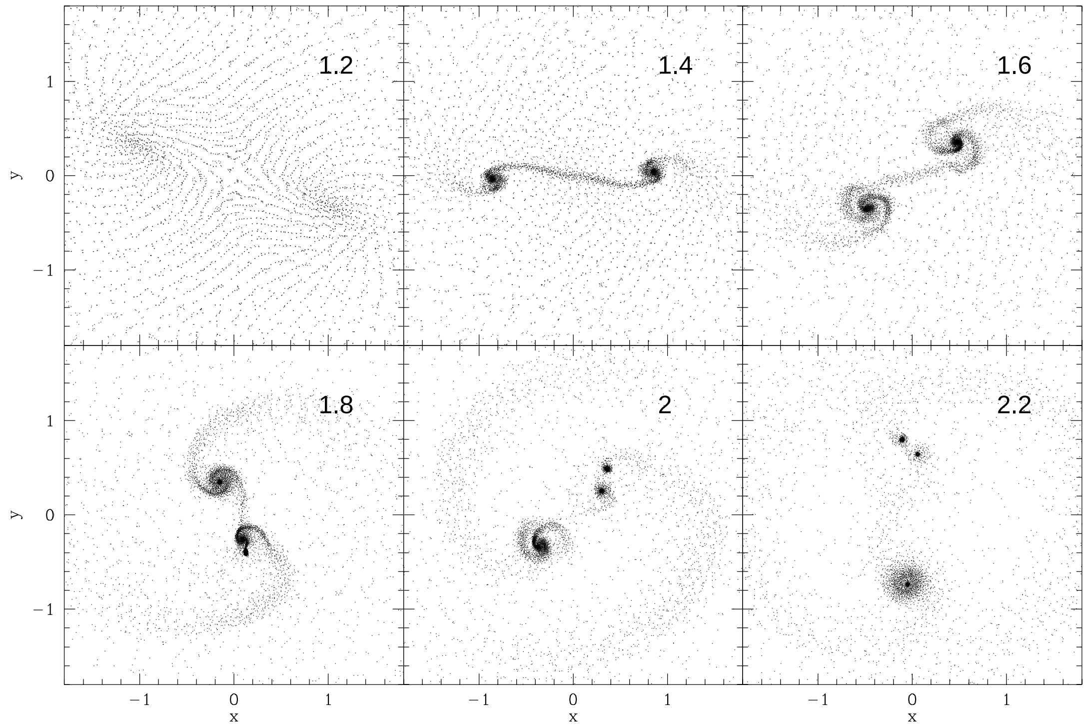

Figure 4.10: The particle positions projected on to the equatorial plane for the Boss & Bodenheimer (1979) standard test case evolved with a polytropic equation of state using standard SPH. In past calculations, the standard test case is typically only evolved to 1.3 $t_{\rm ff}$, however, the use of a polytropic equation of state allows it to be followed further. Collapse of the cloud initially forms two protostars. These two protostars fall toward each other, forming a binary system due to their orbital angular momentum. Subsequently, the fragmentation of the disc surrounding one of the protostars forms a third protostar and a triple system results. The simulation was performed with 8024 particles. The time, in units of the free-fall time ($t_{\rm ff} = 5.52 \times 10^{11}$s), is given in the upper right-hand corner of each panel. The axes are in units of 1.0×10^{16} cm.

The results of Myhill & Boss (1993) were obtained using Eulerian grid codes based on Cartesian (M64) and spherical (B64) coordinate grids. At this stage, the maximum density is $\sim 10^6 \rho_0$. The results are averaged over the two fragments. Fragment mass is calculated from all the particles in one half of the cloud with a density of 100 ρ_0 or greater. The quantities $\alpha_{\rm f}$ and $\beta_{\rm f}$ are then calculated from these particles. The fragment is assumed to be spinning parallel to the z-axis about its centre of mass, rather than about the most dense particle. The specific angular momentum of the fragment $(J/M)_{\rm f}$ is given by the angular momentum of the fragment about the centre of mass divided by the fragment mass. As in Myhill & Boss (1993) this is compared with the specific angular momentum of the initial cloud $(J/M)_{\rm i}$ as a measure of how the initial angular momentum of the cloud is partitioned between the spin and orbital angular momenta of the fragments. Finally, the distance from the fragment's centre of mass to the z-axis D, divided by the cloud radius R, is given. The results are in good agreement with those of Myhill & Boss (1993). The polytropic equation of state does not affect the tabulated fragment properties significantly over the isothermal case (with the exception of α_{f}, due to heating of the high-density gas) as the equation of state only becomes non-isothermal beyond 1.18 t_{ff}.

Following the initial fragmentation of the cloud in Figure 4.10, the fragments (or protostars) continue to fall toward each other due to their lack of angular momentum. However, they do not merge. Instead, the two initial protostars pass each other at periastron at approximately 1.9 t_{ff} and continue to orbit each other. As demonstrated in Table 4.2, the protostars have a high ratio of rotational to gravitational energy. They quickly become bar-unstable, forming spiral arms that move through their discs (Figure 4.10). Before periastron is reached, at 1.79 t_{ff}, the disc around one of the protostars fragments. The cause of this disc fragmentation is the same process as presented by Bonnell (1994). The protostar embedded in the disc is rapidly rotating, making it unstable to the growth of an $m = 2$ bar-mode. In forming a bar, the protostar is able transfer angular momentum to the outer parts of the bar via gravitational torques. These move outward and fall behind the bar, forming spiral arms. Any asymmetry in the two ends of the bar, or their spiral arms, leads to a different rate of angular momentum loss, and hence support, from each side of the protostar. The protostar then contracts non-uniformly, moving its centre of mass away from the centre of mass of the system and spiralling outward. This allows the spiral arms to catch up to one another and they collide. With the mass swept up by the spiral arms travelling through the disc, and the continued infall of material, the collision forms a gravitationally unstable condensation which collapses, forming a secondary. Hence, a triple system is formed.

Although the initial cloud is perfectly symmetric, only one disc has fragmented by 2.2 t_{ff}. This demonstrates that disc fragmentation is a highly chaotic process. Small variations in the particles' positions and velocities in the simulations come from the limited numerical precision of the calculations. These lead to a small amount of asymmetry which allows one disc to fragment before the other. It is highly probable that the gravitational interaction between the two protostars and their discs increases this asymmetry and aids the fragmentation (as suggested in Bonnell et al. 1992). Furthermore, once a close binary is formed, gravitational torques exerted by it on the other disc could help stabilise this disc against fragmentation. Thus, although it is possible to predict that fragmentation is likely to occur from the high ratio of rotational energy to the magnitude of the gravitational energy in the disc, the exact timing and position of the fragmentation are indeterminate. The resulting triple system is a hierarchical system, but may not be stable in the long term. The calculation could not be followed further due to the increasing number of particles contained in the fragments, lengthening the computational time.

In the isothermal case, using a minimum particle smoothing length, the outcome is a quadruple system. In this case, the discs around both initial protostars fragment at approximately 1.54 t_{ff}, well before periastron. The discs fragment earlier than in the polytropic equation of state case because there is less pressure support. With the lack of pressure support, the material must attain more of its support from rotation about the protostars. This decreases the rotational stability of the discs. Also, once spiral arms are formed and collide, the resulting high-density region of gas is more prone to collapse under its self-gravity with an isothermal equation of state than it would be if it were heated. Again the calculation was halted due to increasing computational time at 2.2 t_{ff}.

4.4.2 Evolution with Sink Particles

Although the use of a minimum particle smoothing length or a polytropic equation of state allows fragmentation calculations to be followed further than with a purely isothermal equation of state, the computational time still increases as more particles are accreted by the fragments, and soon becomes unacceptably long. Moreover, with the use of a minimum particle smoothing length, the internal fragment evolution is not followed accurately. Even with the polytropic equation of state, which provides a more physically correct evolution except in the very highest-density regions, the internal evolution of the fragments is not of interest. The main information to extract from fragmentation calculations is which fragments accrete the mass, and what the orbital parameters of the resulting stellar system are. By using sink particles in SPH, the internal evolution can be ignored, increasing the speed of the calculations, and allowing the final result of the fragmentation to be determined.

To ascertain if the use of sink particles in SPH affects the evolution of the cloud outside the fragments, and if so in what ways, the Boss & Bodenheimer (1979) test case was repeated using sink particles of varying accretion radii, with both isothermal and polytropic equations of state. The results from evolving the standard test case with sink particles using four different accretion radii and the polytropic equation of state are presented for comparison with the standard SPH calculation. The accretion radii were 0.02, 0.05, 0.10, and 0.20, in units of 10^{16} cm. The largest radius swallows almost the entire disc around each of the initial protostars. Since a larger fraction of the disc is neglected as the accretion radius increases, only the smallest-accretion-radius calculations might be expected to fragment the discs around the initial protostars. Also, interactions between protostars and discs will be affected in calculations where most of the disc is not modelled, due to the replacement of the disc's gravitational potential with a spherical potential.

Figure 4.11 shows the results of a calculation using the polytropic equation of state and sink particles with boundary conditions and with $r_{\mathrm{acc}} = 0.20$. Two sink particles are dynamically created from the fragments at approximately 1.31 t_{ff}. Most of the volume of the discs that would form around these two sink particles is within the accretion radii, and hence not modelled. Only the very edges of the discs are still visible. Hence, no disc fragmentation occurs, and the result is a binary system. Overall, the dynamics of the calculation are similar to those for the calculation without sink particles. The calculation was followed to 4 t_{ff}. At this stage 79% of the initial cloud is accreted by the

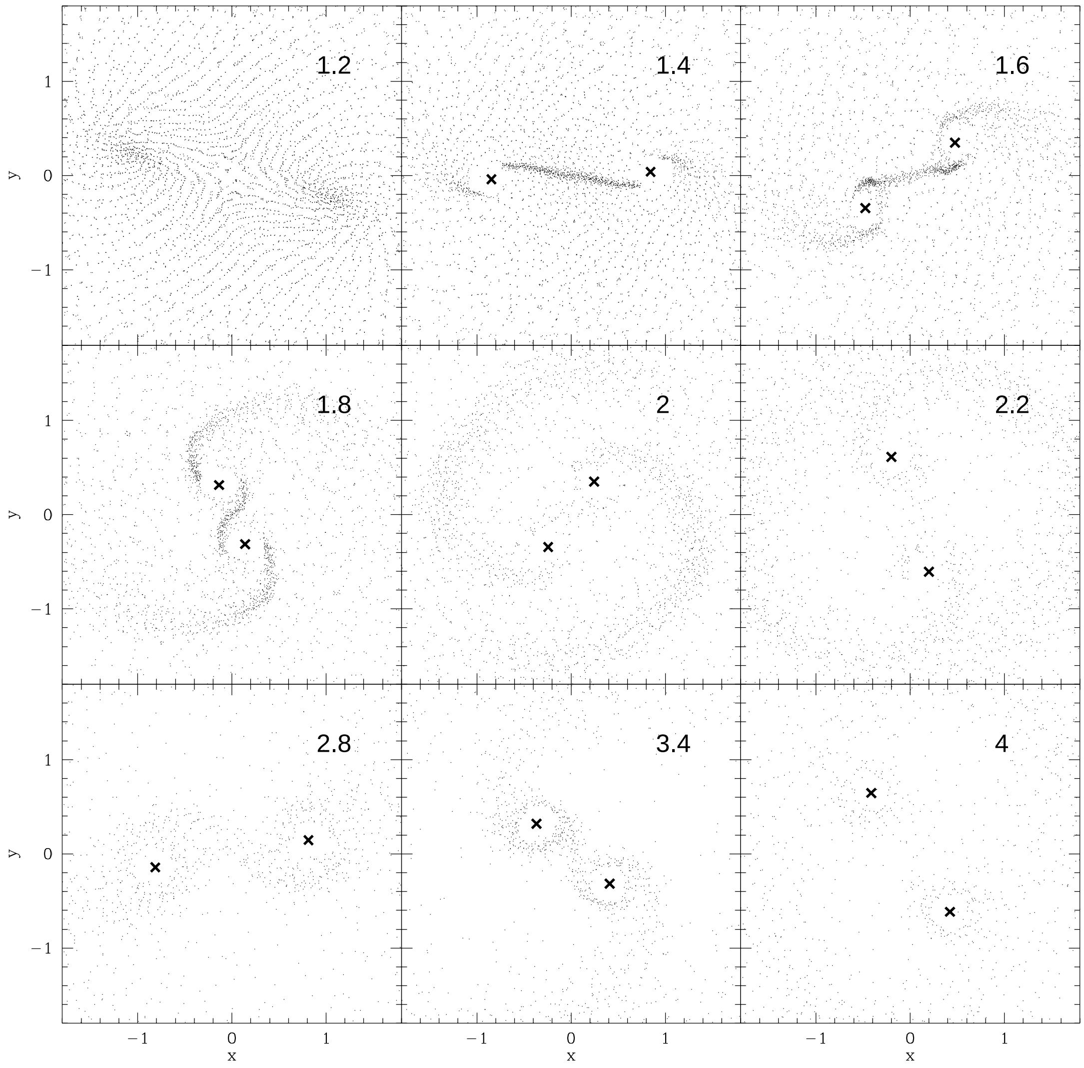

Figure 4.11: The same calculation as presented in Figure 4.10, but using dynamically created sink particles with accretion radii of $r_{\rm acc} = 0.20 \times 10^{16}$ cm. The sink particles are marked with crosses. Global evolution of the system is similar to Figure 4.10, with the details of the calculation within the accretion radii of the sink particles being ignored. The use of sink particles enables the calculation to be followed much further than is possible with standard SPH. The simulation was performed with 8024 particles. The time, in units of the free-fall time ($t_{\rm ff} = 5.52 \times 10^{11}$s), is given in the upper right-hand corner of each panel. The axes are in units of 1.0×10^{16} cm.

sink particles. Most of the rest of the initial cloud material is expelled out to the radius of the initial cloud by gravitational torques from the binary.

Figure 4.12 gives the results of an identical calculation, but with $r_{\rm acc} = 0.02$. In this calculation, most of the material in the discs around the protostars is left intact. The discs do not fragment. Again the evolution was followed to 4 $t_{\rm ff}$ and a binary system results with approximately 80% of the initial cloud being contained by the sink particles, or their surrounding discs, with the rest being expelled out to the initial cloud radius.

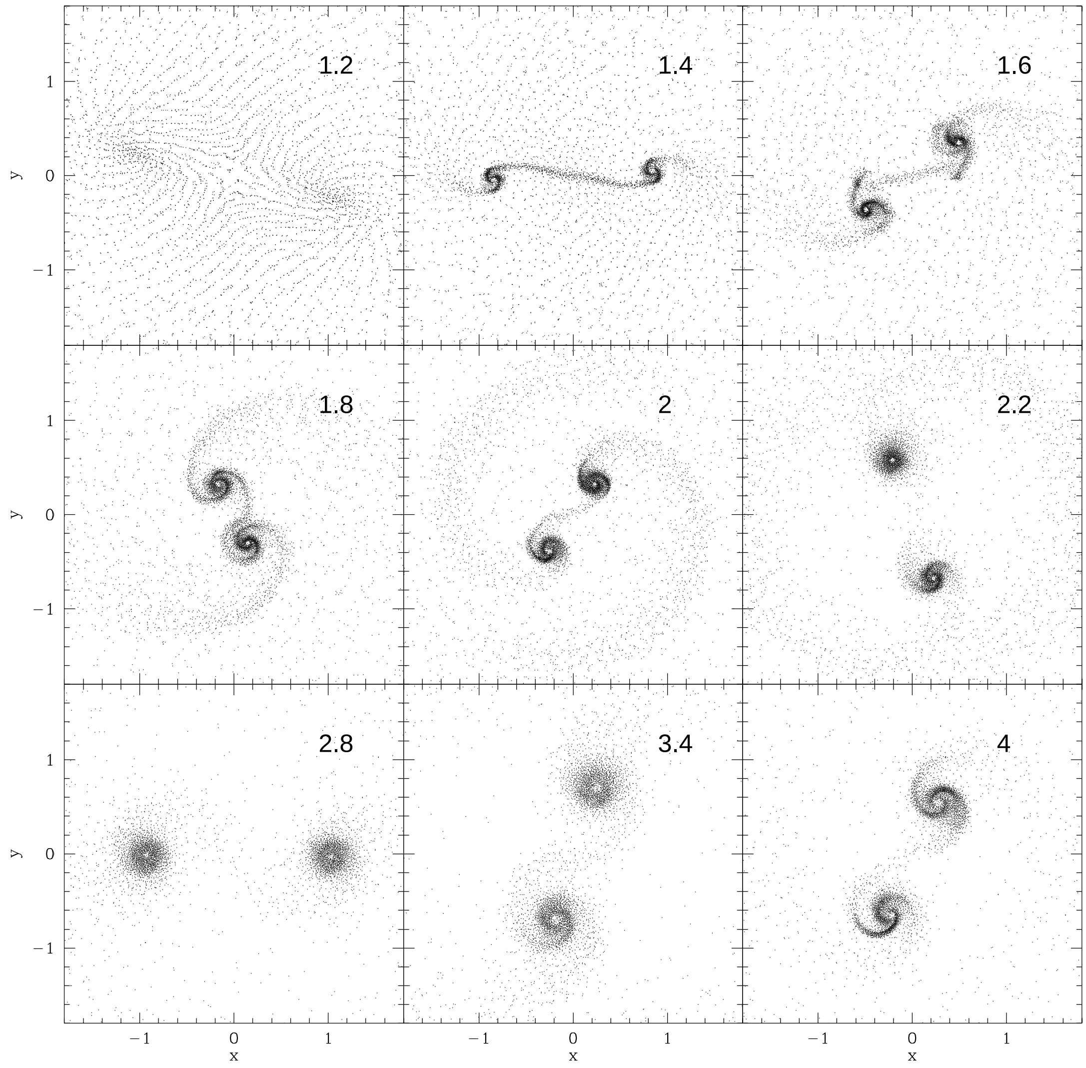

Figure 4.12: The same calculation as presented in Figures 4.10 and 4.11, but using dynamically created sink particles with accretion radii of $r_{\rm acc} = 0.02 \times 10^{16}$ cm. The majority of the disc material for each protostar is outside the accretion radius and is still modelled by the calculation, with the result that the calculation follows the standard SPH calculation closer. The sink particles are not marked, but are contained within the central holes in the protostellar discs. The simulation was performed with 8024 particles. The time, in units of the free-fall time ($t_{\rm ff} = 5.52 \times 10^{11}$s), is given in the upper right-hand corner of each panel. The axes are in units of 1.0×10^{16} cm.

Both this calculation and the larger accretion radius calculation were easily followed further, up to 10 $t_{\rm ff}$, although, the constant-volume boundary conditions at the initial cloud radius gave unphysical results beyond about 4.5 $t_{\rm ff}$.

The dynamics of the gas in the discs in the small-accretion-radius calculations are similar, but not identical, to those of the calculation without sink particles. The evolution is not expected to be identical to the standard SPH calculation for three reasons. First, the gravitational potential of material inside an accretion radius is being approximated by a spherically symmetric distribution, although the error in this approximation should decrease as the accretion radius decreases. Second, the boundary conditions, although being a great improvement over no boundary conditions, are imperfect. The third difference, and perhaps the most important, is that, with the standard SPH calculations, the protostars are kept larger than is physically correct to allow the calculation to be followed. This results in the inner parts of a disc being replaced by a spheroidal protostellar object in approximate solid-body rotation due to the viscosity. This protostar helps to drive the disc fragmentation by becoming bar-unstable itself, as described in Section 1.3.4. With sink particles, this does not occur. There is no central object to aid the fragmentation, and the discs are able to remain in Keplerian rotation right up to the accretion radius. Because of these differences, it is not obvious whether the calculations with small-accretion-radius sink particles, or the standard SPH calculations give more accurate disc evolution. In particular, because the whole process of disc fragmentation is highly chaotic and is determined by the above differences, it is uncertain whether the discs fragment to form close binaries. These calculations show the discs to be highly unstable and likely to fragment, but higher resolution calculations are required to determine whether disc fragmentation actually occurs or not. Regardless, a wide binary is certainly formed.

The orbits of the each of the two initial fragments are given up to 3 $t_{\rm ff}$ for each calculation in Figure 4.13. These were calculated by finding the centres of mass of the sink particles and their discs out to a radius of 0.30×10^{16} cm from each of the initial two sink particles. They are compared with the orbits of the centres of mass of the initial two fragments and their discs formed from the calculation without sink particles. The centres of mass of the initial two fragments have been plotted to avoid the confusion of the fragmenting discs, which is not expected to be followed correctly with such large accretion radii in any case. The only sink particle calculation to give disc fragmentation was the calculation with $r_{\rm acc} = 0.05$, in which both discs fragmented, forming a quadruple system.

The orbits of the initial fragments in Figure 4.13 are all similar until periastron. After periastron the orbits diverge, producing a scatter in the orbits. This is due to the different way each calculation models the interactions between the protostars and discs at periastron. In particular, after periastron, the largest-accretion-radius calculation, in which the protostars and discs are almost entirely contained inside the accretion radii, has a tighter orbit than the second-largest-accretion-radius calculation where parts of the discs are still modelled. For calculations that have parts of the discs modelled outside the accretion radius, the orbits tend to become tighter as the accretion radius decreases and more of the disc is modelled. Two mechanisms are presumably responsible for these effects. The first is the process of angular momentum transport via gravitational torques between the discs' spin angular momenta and the protostars' orbital angular momenta near periastron. The second is the loss of material from the outer edges of the discs which is expelled from the system during the periastron passage. These two mechanisms give a possible explanation for the results. With $r_{\rm acc} = 0.10$, the interaction, via gravitational

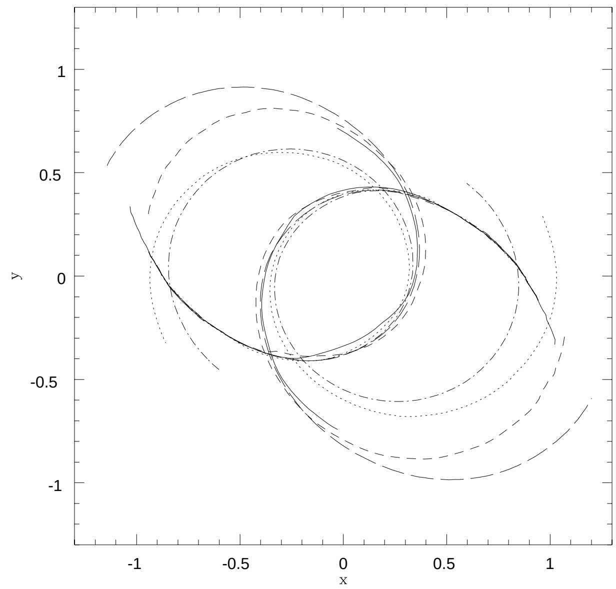

Figure 4.13: The orbits of the centres of mass of each initial fragment formed in the standard test case evolved using sink particles and a polytropic equation of state. The orbits are plotted from 1.3 $t_{\rm ff}$ to 3.0 $t_{\rm ff}$. The sink particles accretion radii are $r_{\rm acc} = 0.02$ (dotted), $r_{\rm acc} = 0.05$ (dashed),$r_{\rm acc} = 0.10$ (long-dashed), and $r_{\rm acc} = 0.20$ (dot-dashed). These orbits are compared to the orbits of the centres of mass, up to 2.2 $t_{\rm ff}$, of the two initial fragments formed in the polytropic equation of state calculation without sink particles (solid line). The centres of mass of the fragments are calculated from all the particles within a radius of 0.30×10^{16} cm from the initial sink particle (or the densest particle for the standard SPH calculation) of each fragment. It is noted that the discs around both the initial sink particles in the $r_{\rm acc} = 0.05$ calculation fragmented to form close binaries, and in this case both sink particles in each of the close binaries were used for the centre of mass calculation. The initial cloud free-fall time $t_{\rm ff} = 5.52 \times 10^{11}$s. All distances are in units of 1.0×10^{16} cm.

torques, of the protostars with the discs, which are rotating more quickly, transfers angular momentum from the discs' spin angular momenta to the orbital angular momenta of the protostars. This gives a larger orbit than the case with $r_{\rm acc} = 0.20$ where there can be no such interaction. For the cases where the disc is modelled outside the accretion radius, the decreased apastron separation as the accretion radius is reduced may be due to greater loss of material from the edges of the discs from the system at periastron. The spiral arms passing through the discs act via gravitational torques to move angular momentum further out in the disc. With more of the disc modelled, the outer disc material may be expected to acquire more angular momentum from the inner parts of the discs, resulting in more material being expelled by the binary at periastron as the edges of the discs are disrupted. The loss of the orbital angular momentum of the system in expelling this material could give the tighter orbits with decreasing accretion radius seen in Figure 4.13, since more material is expelled. This mechanism may help to explain the observed absence of medium-period, high-eccentricity binary systems in stellar surveys (Duquennoy & Mayor 1991). These interactions between protostars and discs require further study.

In summary, for each calculation, the global results are the same. In all cases a binary system is formed with each component containing approximately 40% of the original cloud mass at 4 $t_{\rm ff}$. The remainder of the mass is expelled, by the binary, beyond the initial cloud radius. The orbits, until periastron, are essentially independent of the accretion radius used. However, at periastron approach, interactions between the protostars and the discs require that the discs be resolved if the evolution of the system is to be correctly followed. In addition, each of the binary components either consists of a protostar surrounded by a disc, or may itself consist of a binary, if the discs surrounding the initial protostars fragment. The use of sink particles allows the calculations to be followed to completion in a realistic amount of computational time. The polytropic equation of state calculation without sink particles requires 20 days of Sun Sparcstation 5 CPU time to evolve it to 2.2 $t_{\rm ff}$, whereas with sink particles the calculations take between a half a day and two days to reach the same point, depending on the size of the accretion radius that is used. Moreover, the calculation time is constantly decreasing with sink particles due to the decreased number of active particles, whereas the time is constantly increasing without sink particles as more particles join the protostellar fragments. Hence, sink particle calculations can be evolved until all of the initial cloud material has been either accreted or expelled from the system.

Finally, the Boss & Bodenheimer (1979) sink particle calculations evolved with an isothermal equation of state allow disc fragmentation to occur far more easily than with the polytropic equation of state, and the discs around each of the initial protostars fragment early in the calculation even with the largest accretion radius of $r_{\rm acc} = 0.20$. It is clear that the initial result is still a binary system whose parameters are similar to those given by the polytropic equation of state calculations. However, each of the initial components of the binary itself consists of a closer binary and the separations of these closer binaries are often not small enough for the system to be a stable hierarchical system.

4.5 Conclusions

A new method for extending molecular cloud fragmentation calculations beyond protostar formation has been presented. It allows these calculations to be followed for as long as is required for all the initial cloud material to be either accreted by the protostars, or expelled from the system. This is achieved by using an SPH code where each protostellar fragment that forms during the collapse of a molecular cloud is replaced by a single, non-gaseous particle. This particle accretes infalling material within a specified radius, and is surrounded by appropriate boundary conditions to avoid the presence of the accretion hole adversely affecting the dynamics of material outside the accretion zone. In this way, the time steps required to evolve the calculations are kept large enough that the final state may be reached.

As a demonstration of this technique, the Boss & Bodenheimer (1979) standard isothermal test case for the fragmentation of a molecular cloud has been evolved until approximately 80% of the initial cloud is contained in the protostars, or their surrounding discs, and the rest of the material has been expelled out to the radius of the initial cloud. It is found that a wide binary system is formed, with roughly equal mass components. Each component may itself consist of a close binary system due to the fragmentation of the discs that form around the two initial protostars, depending primarily on how the equation of state of the material is treated after it becomes optically thick.

Using this new technique, comparison between the results of cloud fragmentation calculations and the observed characteristics of pre-main-sequence and main-sequence stellar systems is now possible, as the fragmentation calculations can be followed long enough to obtain the final state of the system. This method can also be applied to many other problems where gas dynamics around massive objects is to be studied.